RANS and LES simulations at partial load in Francis turbines: Three-dimensional topology and dynamic behaviour of inter-blade vortices

François Doussot, Guillaume Balarac, James Brammer, Yann Laurant, Olivier Métais

International Journal of Fluid Machinery and Systems
Vol. x, No. x, October-December 20xx

DOI: 10.5293/IJFMS.20xx.x.x.xxx
ISSN (Online): 1882-9554

Original Paper

RANS and LES simulations at partial load in Francis turbines: Three-dimensional topology and dynamic behaviour of inter-blade vortices

F Doussot[1], G Balarac[1], J Brammer[2], Y Laurant[2], O Métais[1]

[1]Univ. Grenoble Alpes, CNRS, Grenoble INP, LEGI, 38000 Grenoble, France
francois.doussot@univ-grenoble-alpes.fr
[2]GE Renewable Energy, Hydro Solutions, 82 Avenue Léon Blum, 38041 Grenoble Cedex 9, France

Abstract

Hydraulic machines are designed to operate in flow conditions close to the best efficiency point. However, to respond to the increasing demand for flexibility mainly due to the integration of renewable energy in the electric grid, the operating range of Francis turbines has to be extended towards smaller discharge levels without restriction. When Francis turbines are operated typically between 30% and 60% of the rated output power, the flow field is characterized by the appearance of inter-blade vortices in the runner. In these off-design operating conditions and due to these phenomena, dynamic stresses level can increase, and potentially lead to fatigue damage of the mechanical structure of the machine. The objective of this paper is to present investigations on the dynamic behaviour of the inter-blade vortices and their impact on the runner by using numerical simulations. Computations were performed with different turbulence modelling approaches to assess their relevance and reliability: Reynolds-Averaged Navier-Stokes (RANS) and Large-Eddy Simulation (LES). Computations aimed to better understand the emergence condition of the inter-blade vortices. The analysis showed that vortices can be generated due to poor inlet adaptation at part load, however other vortices can also be due to a local backflow in the runner. The competition between these both phenomena leads to various topologies of the inter-blade vortices. The numerical results were compared to experimental visualizations performed on scaled model as well as to previous numerical studies results. The impact of these inter-blade vortices on the runner were also investigated by considering the pressure fluctuations induced on the blades. The dynamic loading on the blade has to be known in order to evaluate the lifetime of the runner by mechanical analysis. Different operating conditions have been simulated to understand how the pressure fluctuations depend on the operating conditions. The localization of the pressure fluctuations and their consequences on the frequency signature of the torque fluctuations have been analyzed. This article is presenting a part of the work presented at the 29th IAHR Symposium on Hydraulic Machinery and Systems, Kyoto, 2018 [1], and presents another vortex topology and a comparison of LES results of several operating conditions.

Keywords: Inter-blade vortex, Channel vortex, Part load, Francis turbine, Large Eddy Simulation

1. Introduction

The recent development of new renewable energy technologies, such as wind and solar, leads to an uncontrolled amount of energy dispatched. The need for flexibility is brought by their integration in the grid. Supply and demand has to be kept in balance in real time to guarantee electric grid stability [2].

Hydroelectric power therefore has a major advantage in the regulation of the power supply compared to other technologies. Hydro energy sources can respond in few seconds. But flexibility is not only a matter of time response, but also a matter of amount of energy produced. For hydroelectric power, this flexibility can be brought by operating in a wide range of flow conditions, especially using flow rates smaller than usual. But these off-design operating conditions can lead to the appearance of secondary flow phenomena. This turbulent flow field could generate pressure fluctuations in the machine. This paper deals with Francis turbines, which are the most widely used type of hydro turbine with about 60% of the global hydropower capacity in the world.

Received January 15 20xx; revised March 20 20xx; accepted for publication June 20 20xx: Review conducted by Prof. Soon-Wook Kim. (Paper number O10xxx) (This information will be given when accepted.)
Corresponding author: François Doussot, PhD student, francois.doussot@univ-grenoble-alpes.fr

*This article is presenting a part of the work presented in the paper [1] that has been discussed at the 29th IAHR Symposium on Hydraulic Machinery and Systems, Kyoto, 2018.

In part load conditions, a vortex rope can be seen in the draft tube cone. For lower discharges, with an output power roughly between 30% and 60% of the nominal value, inter-blade vortices can appear in the runner. At these operating conditions, an increase in pressure fluctuations in the runner can be observed, which could cause fatigue damage on the mechanical structure.

Inter-blade vortices have been studied for several years using numerical and experimental approaches; however the sources and the driving phenomena of the vortices have not been fully understood. Away from the design point, the flow field entering the runner is misaligned with the geometry of the blades. Wack [3] suggests that this poor incidence angle generates the inter-blade vortices. Zhou et al. [4] also studied the occurrence and the location of the vortices depending on the operating point. According to their study, the mechanism of this phenomenon is driven by the reverse flow near the hub and is not related to the incidence angle. Yamamoto [5] presents similar results: a numerical simulation shows a significant backflow region at the center of the draft tube cone. Flow analysis in the runner shows that this backflow region plays a major role in the formation of the inter-blade vortices. In another numerical investigation, Zhou et al. [6] show with RANS computations and k-ω SST model that the vortex related to the reverse flow is the most prone to cavitation. Moreover this article suggests a classification of the inter-blade vortices appearing in the runner into four types. According to this study, they can be due to the incident angle, to a cross-flow occurring on the blade pressure side, to the geometry at the junction between the leading edge and the shroud, or finally to the reverse flow.

These off-design conditions can increase dynamic stresses on the blades. Bouajila et al. [7] has shown that these flow regimes are characterized under certain operating conditions by pressure fluctuations on the blades with a high and wide-band frequency signature. This hydraulic phenomenon could potentially cause fatigue damage and reduce the lifetime of the turbine. However this frequency signature has never been predicted by numerical simulations and its origin is still not well understood.

The analysis presented in this paper was conducted on a 17 blades low head Francis turbine, with a distributor composed by 24 guide vanes and 24 stay vanes. An experimental study was previously performed in the GE Hydro Laboratory [8]. The visualisations of the cavitating vortices and on-board pressure measurements have been compared with the numerical results.

The first part of this paper describes investigations on the topologies and causes of the vortices thanks to steady simulations. In a second part the link between pressure fluctuations and the topologies of the vortices and their influence on the torque fluctuations have been analysed. Large eddy simulations (LES) were used in order to resolve most of the turbulent length scales in order to understand the different phenomena appearing in the runner.

2. Characterization of the inter blade vortices using steady simulations

RANS simulations were computed using the solver CFX to study the mean flow of a wide range of operating conditions thanks to their low computational cost.

Operating points were described by their reduced velocity $n_{11} = \frac{nD}{\sqrt{H}}$ and the reduced discharge $Q_{11} = \frac{Q}{D^2\sqrt{H}}$. Q is the flow rate, D the outlet diameter of the runner, n the runner speed and H the net head. A reduced discharge can be defined by $\varphi = \frac{V_m}{U}$ were Vm and U are respectively the meridional and the circumferential velocity at the outlet surface of the runner. φ is normalised by its value at the best efficiency point, defining the non-dimensional value $\overline{\varphi}$.

2.1 Numerical setup

The computational domain has been reduced to a single blade and guide-vane channel using periodic boundary conditions to reduce the simulation time. The draft tube was not included in the simulation. However, as part load operating conditions are characterized by a back-flow in the outlet of the runner, in order to avoid a strong interaction between the outlet and the recirculation zone the cone section was virtually extended. Furthermore, to ensure model convergence, a constant flow rate was used as the outlet boundary condition and a constant total pressure set at the inlet. The Shear-Stress-Transport turbulence model has been chosen. Initial tests showed a strong mesh sensitivity. Therefore, a refined structured mesh of 2.3 million nodes was used to correctly discretize the vortices, leading to a dimensionless wall distance y^+ around 2 in the runner, with a maximum of 5 near the shroud.

The value y^+ has to be close to 1 to resolve the boundary layer in order to estimate correctly the losses. The operating points are characterized by their n_{11} and Q_{11} values. As n_{11} and Q_{11} values depend on the head, which is a result of the simulation, an iterative method has been used. The net head was estimated using the results of the CFD calculations for the runner torque and head loss, combined with assumed analytical values for the other components not included in the simulation.

2.2 Validation of the model

The numerical results were validated using the experimental data. A good agreement on the torque was reached, with an over-estimation between 5 to 10% of the torque. This over-estimation could be expected because some experimental losses were not considered in the simulation, such as the disk friction losses.

Assuming that the presence of cavitation would not change the location of the vortices, experimental and numerical results can be compared. The CFD simulations in this study used a single-phase model. Therefore, the vortices have to be identified using a suitable criterion. Among the criteria suggested in [9], an iso-surface of Q-criterion has been used to identify coherent vortices, because this criterion is particularly adapted to the identification of large scale vortices in a turbulent flow.

The results show a good prediction of the location of the vortices, as shown on Fig. 1 and Fig. 2. The corresponding operating points are identified on a reduced hill chart in Fig. 4. The location of the cavitating vortex depends on the operating condition. It can be attached to the leading edge such as in Fig. 1, or to the hub as shown in Fig. 2. Other operating points have been compared, showing also relevant vortex location prediction.

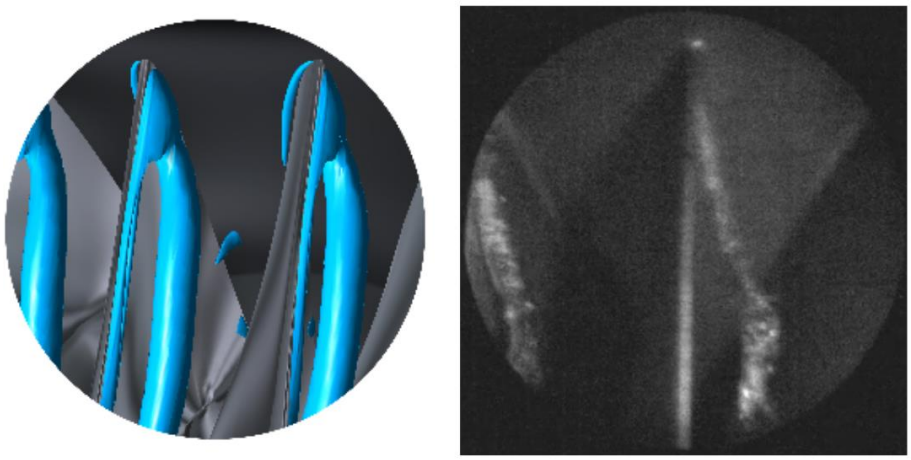

(a). Iso-Q-Criterion **(b)** Experimental cavitation visualization

Fig. 1 Comparison between numerical and experimental results at OP1.

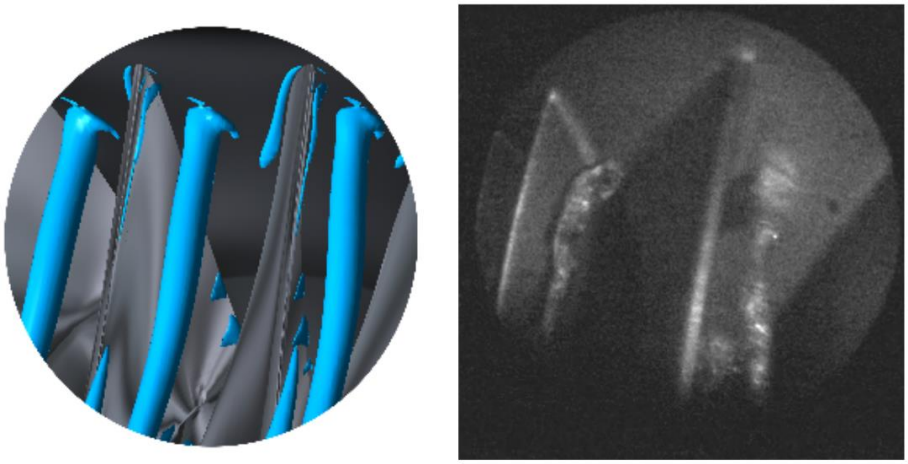

(a). Iso-Q-Criterion **(b)** Experimental cavitation visualization

Fig.2 Comparison between numerical and experimental results at OP5.

2.3 Four types of vortices

The previous observations have shown different topologies of inter-blade vortices, as shown in Fig. 3. In order to understand their driving phenomena, the inter-blade vortices can be classified into four categories.

Reverse flow vortices:

Small discharges correspond to small inertia of the fluid. Therefore the centrifugal force keeps the incident flow at the periphery of the runner. It creates a depression at the runner outlet, underneath the runner tip, leading to a large recirculation zone.

This backflow is driven on the suction side of the blades by the Coriolis force. The interaction between the incident flow and this backflow generates a shear flow, which creates the inter-blade vortex. The greater the backflow, the closer the vortex is to the leading edge. This type of vortex, shown in Fig. 3a, appears independently from the following vortices. This result matches one of the vortices characterized by Zhou et al. [4]

Incidence vortices at the suction side:

Deep part load operating conditions are characterized by small opening of the guide vanes. Then, the flow field at the inlet of the runner is strongly misaligned. These vortices are also already presented in the literature [6].

The RANS simulations show that the strong shear stress in the vaneless space has a major impact on the incident flow. In these operating conditions, the direction of the fluid changes completely in the vaneless space. The flow angle at the leading edge is different from the one given by the guide vanes. Especially for low n_{11} values, the incident angle generates a flow separation on the suction side. As the meridional velocity in the vaneless space is the smallest closed to the hub, this flow separation appears at first closed to the hub. The Coriolis force then brings back the stalled streamlines to the suction side, generating the vortex. Therefore, this type of vortex is attached to the leading edge, as shown in Fig. 3b.

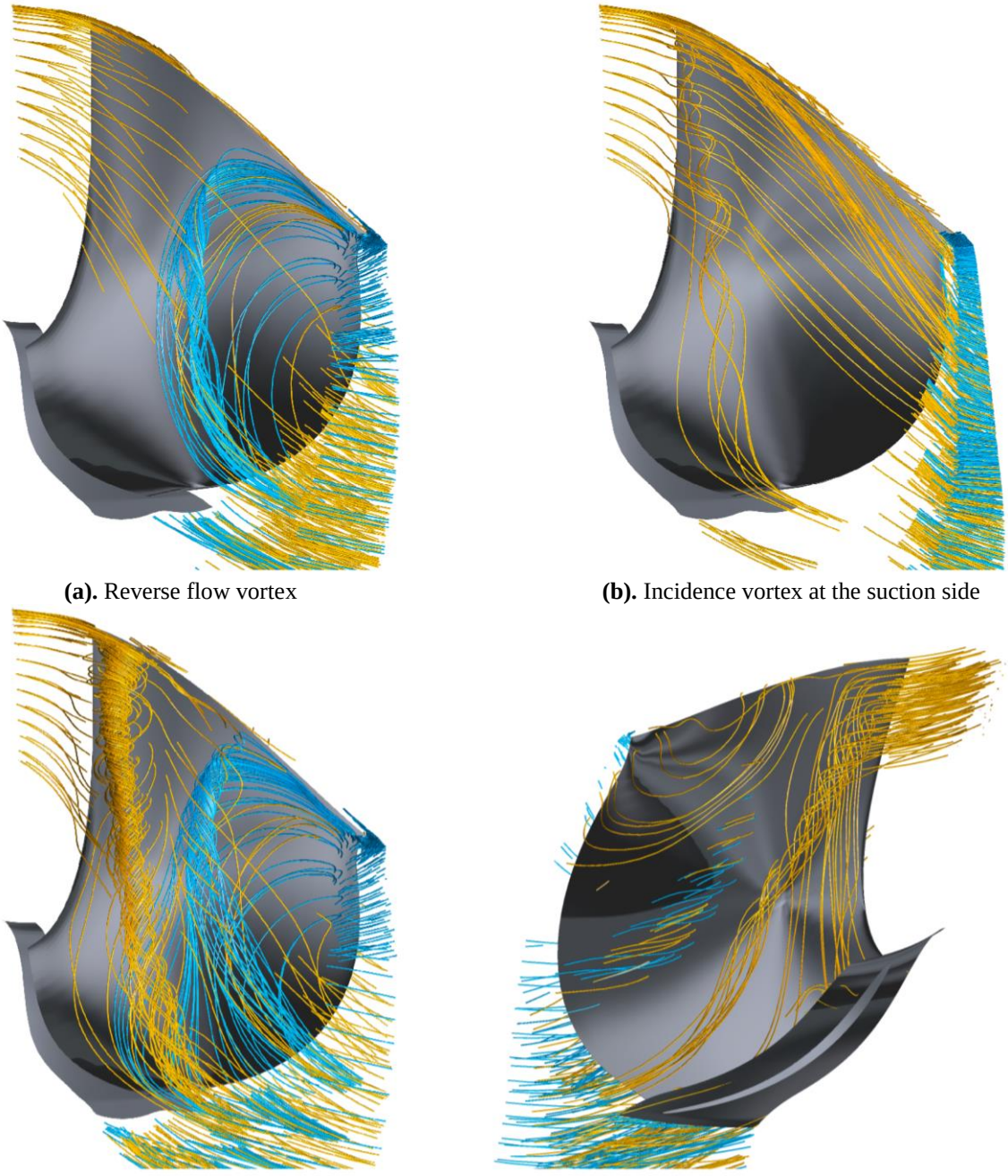

(a). Reverse flow vortex

(b). Incidence vortex at the suction side

(c). Generalized incidence vortex (yellow streamlines) at the suction side

(d). Incidence vortex at the pressure side

Fig. 3 Four types of vortices with the velocity streamlines: the yellow ones come from the inlet and the blue ones from the outlet.

Generalized incidence vortices:

This third category is a degraded form of the previous phenomenon. In this case, the flow separation appears on a large part of the leading edge and cannot be advected by the incident flow. As the separation zone creates a vertical stall region after the leading edge, the streamlines swirl around vertical axis closed to the edge. Thus this type of vortex is attached to the hub and takes a large part of the channel. Figure 3c shows this phenomenon. To our knowledge, this vortex topology has never been described in the literature.

Incidence vortices at the pressure side:

This last type of vortex appears for high n_{11} values. In these regimes the rotational velocity of the runner is relatively too high compared to the orthoradial velocity of the flow at the leading edge. Then a flow separation appears at the pressure side of the runner, creating a stall region. This flow separation is advected by the mean flow, which creates the vortex.

Thus this type of vortex is attached to the leading edge of the channel. As the second type of vortex, it appears at first closed to the hub. Figure 3d shows this phenomenon.

A small vortex in the junction between the leading edge and the shroud, identified by Zhou et al. [6] as another type of vortex, has also been observed for all the operating points.

2.4 Which vortices for which operating condition?

According the previous classification, each type of vortex is associated to a physical phenomenon. These phenomena depend on the operating conditions of the machine, and can be identified on the hill chart. Thanks to the low cost of the RANS simulations, many operating points can be simulated. In order to explore the entire part load conditions, a wide range of n_{11} and Q_{11} values have been used. Five values of n_{11} have been chosen, using each eight values of Q_{11}. Several points with lower and higher values of n_{11} have been added to extend the simulated range. The results are presented on a typical $\{n_{11}, Q_{11}\}$ hill chart in Fig.4. The limits presented here correspond to the case where the velocity streamlines begin to swirl. There is no link between these limits and the appearance of cavitation or mechanical stress.

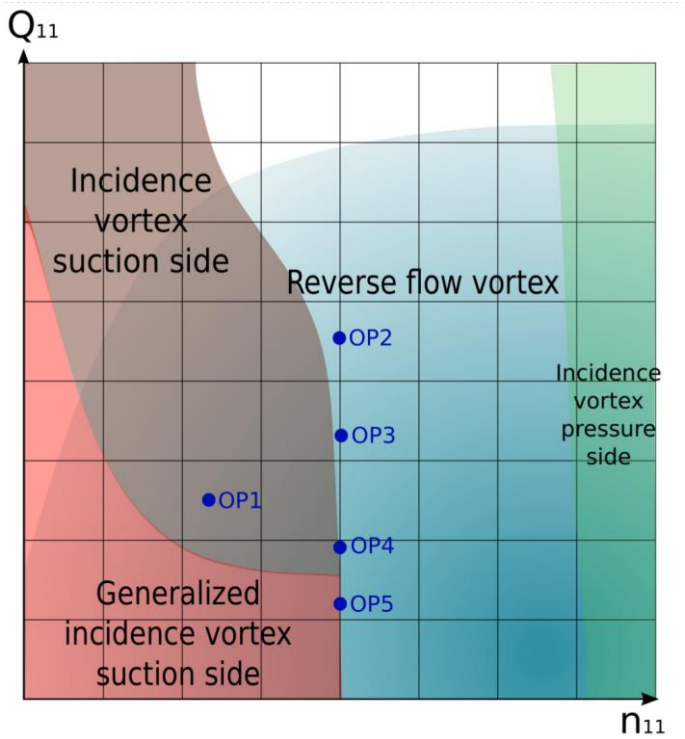

Fig. 4 Types of vortices at part load conditions depending on the operating point.

The vortex created from the reverse flow appears for most of the part load operating points. However, for high Q_{11} values, this vortex is very small and stays close to the trailing edge. The incidence vortex is due to the poor adaptation of the fluid angle at the leading edge. It appears that this vortex is generated for low n_{11} values. These first two vortices can appear in the runner at the same time. Their structures can be merged into a single vortex in the inter-blade channel. The limit between reverse flow vortices and generalized incidence vortices is not clear. When the reverse flow is strong enough to go back to the leading edge the created vortex makes the incident flow separate from the blade. Therefore, these two types of vortices share the same topology for low Q_{11} values: a large vortex attached to the hub can be expected.

This observed behaviour is likely to differ with other blade geometries; however the exact impact of design parameters on the vortex formation is still not fully understood. RANS simulations are able to approximately evaluate the topology of the vortices according the operating point. But no information about the dynamic behaviour of the flow field in the runner, especially about the pressure fluctuations on the blade, can be brought by these simulations.

3. Large eddy simulation of the dynamic pressure fluctuations depending on the type of the operating condition

3.1 Numerical setup

LES can be used for such industrial test cases. The biggest scales are explicitly resolved while the smaller scales, more universal, are modelled using a subgrid scale model. LES simulations have been run in solver YALES2 by using the dynamic Smagorinsky model [10]. It uses a finite volume method and a fourth order scheme. The incompressible solver has been chosen for this test case. The maximum Courant number is set to 1.

As in RANS simulation, a single runner channel has been modelled. Periodic boundary conditions have been used, assuming that this phenomenon only depends of the dynamic behaviour of each channel. A similar extension of the domain has been used to improve the modelling of the reverse flow in the draft tube cone. A mesh sensitivity study has been led. Finally a uniform tetrahedral mesh composed of 50M cells has been used. This mesh is shown in Fig. 5. It is assumed that the boundary layer has not a major influence on the topology of the vortices and the pressure fluctuations there are generating. As this work is focused on the dynamic behaviour of the vortices, no wall refinement was made, leading to a y^+ value of about 35 in the runner.

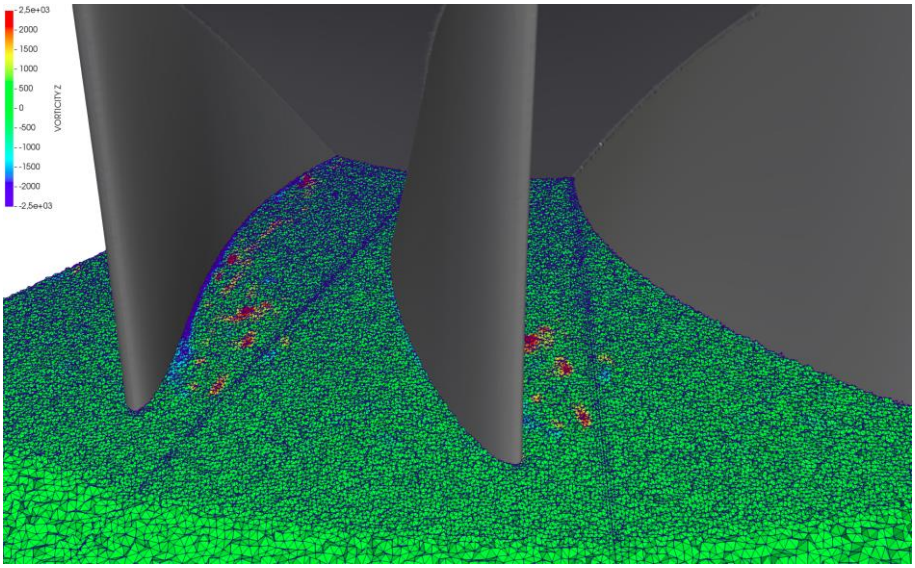

Fig. 5 Horizontal slice of mesh in the runner colored by the axial vorticity, rotated for the visualization.

The solution has been solved in the rotating frame. The velocity field has been imposed at the inlet boundary condition which corresponds to the outlet flow at the guide vanes exit. This velocity field has been extracted from a RANS calculation including the guide vanes, the runner and the draft tube. The velocity components have been averaged circumferentially. The torque was accurately predicted with errors lower than 15% for all the operating points investigated. The numerical spectra are made from 25 runner revolutions, initialized with a converged solution.

3.2 Comparison of the vortex topologies between RANS simulations and LES

LES are used to study the dynamic behaviour of the inter-blade vortices. However it also provides also information about their topologies and their localization that can be compared with RANS solutions.

Whilst LES and high performance computational resources enable to perform high-fidelity simulations, it generates a large amount of data making it difficult to extract relevant information regarding the large-scale phenomena. Visualization of Q-criterion with LES simulation is more prone to show smaller structures, making the visualization of relevant topologies very difficult. Therefore, high order filtering based on the mesh size has been used to filter the smaller vortices and to visualize only the big scales of the structure [11]. As LES needs a lot of computational resources, a limited number of operating points have been studied. The results are illustrated for OP2 and OP4.

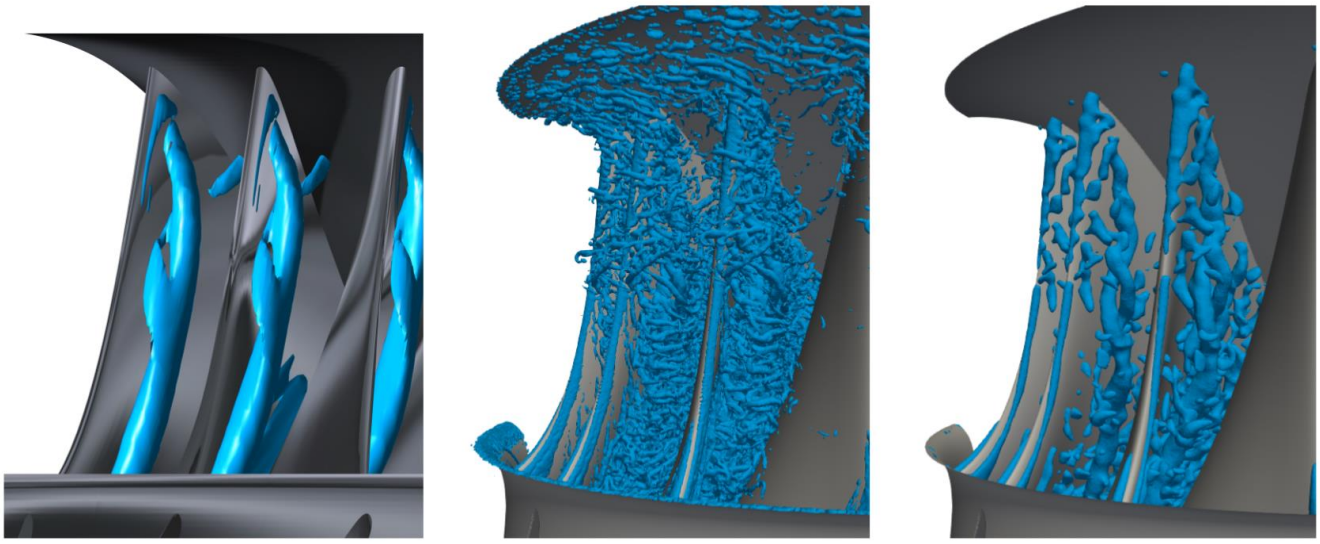

(a). RANS Q-Criterion **(b).** LES Q-Criterion **(c).** LES filtered Q-Criterion

Fig. 6 Comparison between RANS and LES results at OP4.

The location of the vortices is similar for OP4, as shown in Fig. 6: in both cases, the reverse flow vortex and the incident vortex merge in a single vortex close to the leading edge. However, as shown in the Fig. 6b, LES predict a lot of small turbulent structures stretched around the vortex.

Figure 7 presents the same comparison at OP2, for a higher Q_{11} value. Steady results clearly show the reverse flow vortex in Fig. 7a and did not predict any flow separation at the leading edge. LES result shows small structures emerging from this edge in Fig. 7b. With the filtering operation, Fig. 7c shows the reverse flow vortex at a similar location than the RANS calculation.

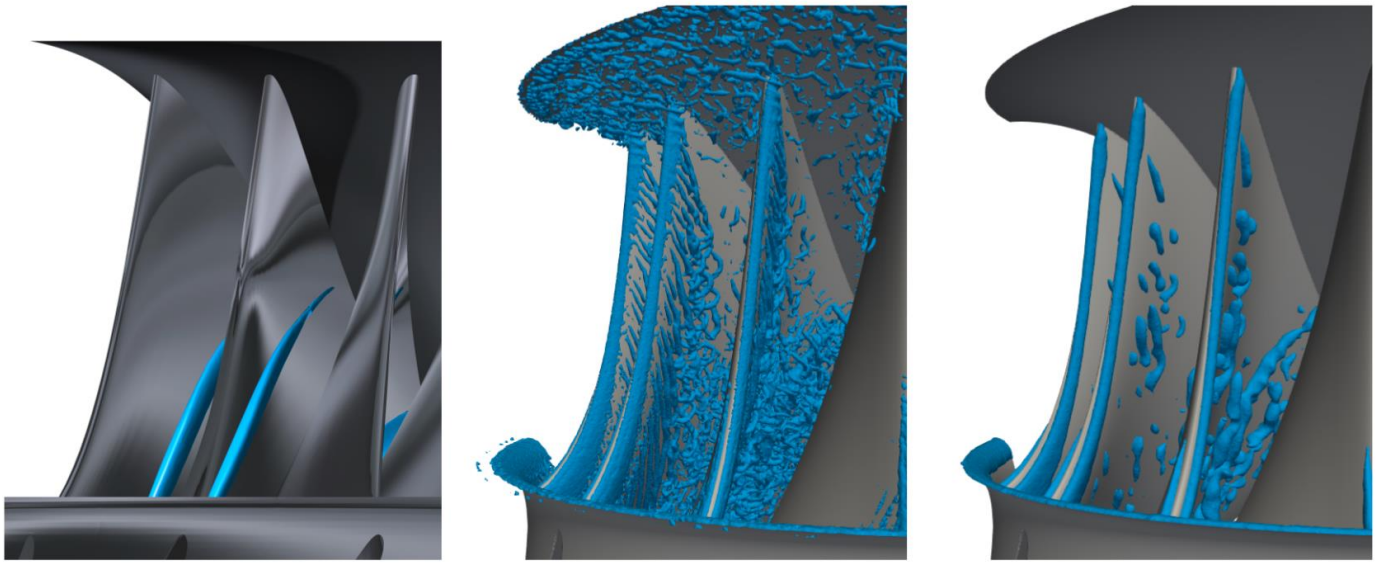

(a). RANS Q-Criterion **(b).** LES Q-Criterion **(c).** LES filtered Q-Criterion

Fig. 7 Comparison between RANS and LES results at OP2.

This brief comparison shows that the results are similar in terms of topology between the RANS simulations and LES. However the delimitation of the different types of vortices defined in Fig. 4 with RANS simulations can slightly change depending on the turbulence model.

3.3 Dynamic behaviour of the inter-blade vortices depending on the operating points

The aim of this section is to understand how the pressure fluctuations induced by the vortices are depending on the operating conditions. The localization of the pressure fluctuations is going to be discussed in a first part, and then the frequency signature of these fluctuations are going to be investigated. Four operating points are studied here, OP2 to OP5, corresponding to a fixed n_{11} value in order to understand the influence of n_{11} on the pressure fluctuations.

Localization of the pressure fluctuations depending on the operating points:

Unsteady simulations allow to investigate statistical physical quantity, such as RMS values of the pressure. Figure 8 shows the pressure RMS values on the runner and on a horizontal plane representing the mean velocity vectors in the channel for each operating point. These visualizations show that the pressure fluctuations mainly appear at the suction side of the blade where inter-blade vortices occur.

This figure firstly shows that the pressure fluctuations in the channel mainly increase when Q_{11} decreases. Secondly it clearly demonstrates that these pressure fluctuations are generated by the flow separation. Indeed, OP2 shows a small flow separation at the leading edge, as discussed in the first part. The pressure fluctuations appear in this region due to the unsteady behaviour of the flow separation as shown by the velocity vector in Fig. 8a. The operating point OP3 shows a similar flow separation and the linked pressure fluctuations. However the reverse flow vortex is reaching the represented plane. The fluctuations are more important in this region, showing that the reverse flow vortex in this case is more unsteady than the incidence vortex. While in this plane OP3 shows two separate vortices, the two vortices are merged at OP4 because of a stronger reverse flow vortex as shown by the velocity vectors in Fig. 8c. This vortex is then characterized by strong pressure fluctuations at its center. However not a big rise in the pressure fluctuations on the blade can be noticed. Finally OP5 is characterized by higher pressure fluctuations at the center of the vortex and in the reverse flow area. The pressure at the center of the vortex is actually lower than at OP4: its motion generates consequently higher pressure fluctuations. The streamwise motion of the vortex can be guessed looking at the shape of the maximum pressure fluctuation zone in Fig. 8d.

In these three last cases, the reverse flow appears to be particularly unsteady. The fact that these simulations are considerably simplified has to be underlined; just the dynamic of the vortices are investigated here. In these operating conditions, many other phenomena could generate pressure fluctuations in the machine and are not considered in this model.

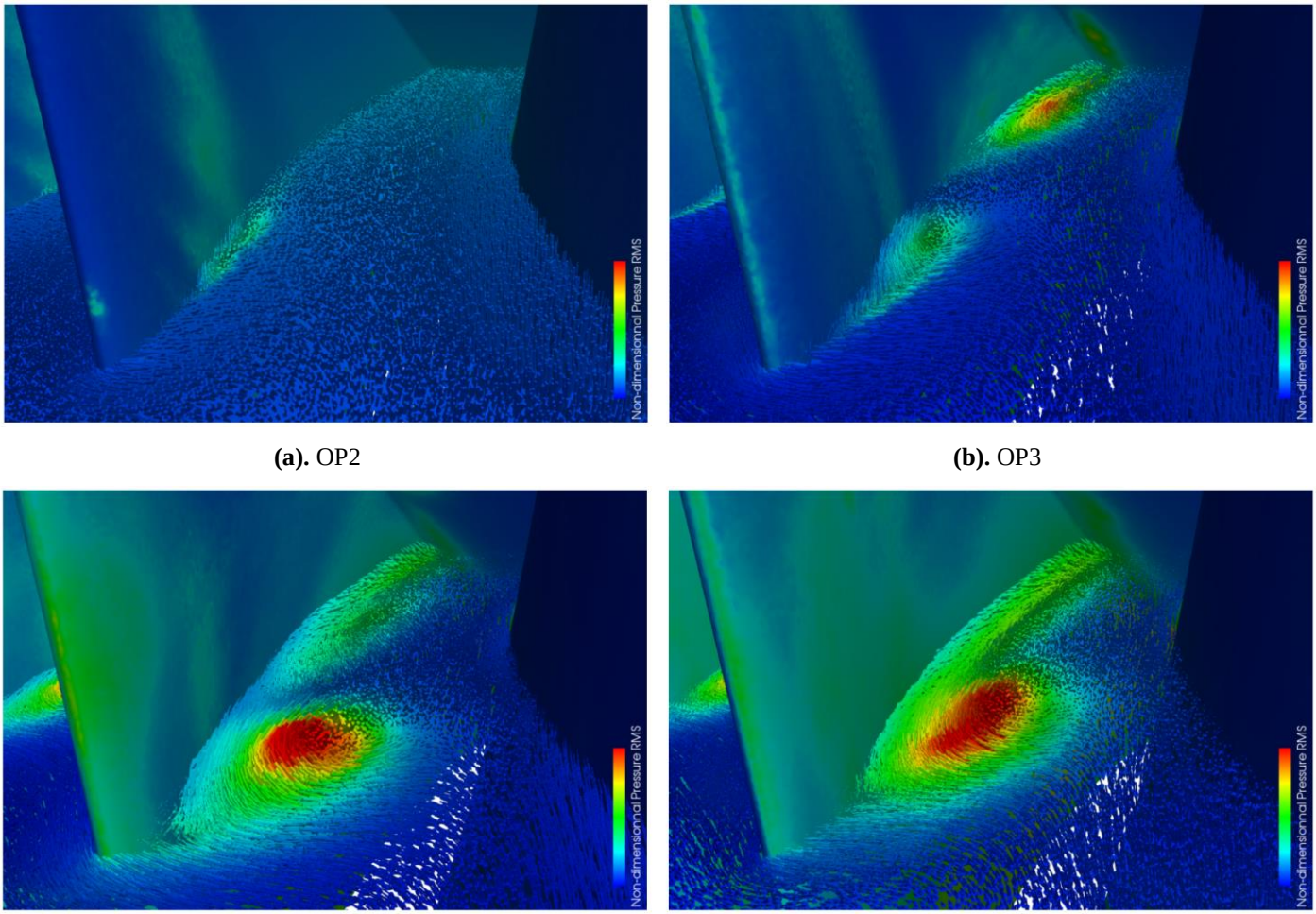

(a). OP2 **(b).** OP3

(c). OP4 **(d).** OP5

Fig. 8 Pressure fluctuations on the blades and in the channel at OP2 to OP5.

Frequency of the pressure fluctuations depending on the operating points

Once the link between pressure fluctuation and inter-blade vortices has been established, the frequency components of the fluctuations can be investigated. The objective is to make a quantitative analysis of the unsteady phenomenon occurring in the runner.

As the pressure pulsations on the blades could generate the fatigue damage of the runner, pressure signal are usually used to analyze the dynamic loading on the blades. However, as shown in the previous part, the localization of the pressure fluctuations differs from one operating point to another. Then, to measure a comparable physical quantity, the torque fluctuations can be analyzed. Indeed, the torque is mainly due to the pressure force on the blade, and then the torque fluctuation is a good indicator of the pressure fluctuations on the entire runner. The mean torque decreases as shown in Fig.9 a with the flow rate. This figure also point out that the standard deviation of the torque has the opposite behaviour: it increases when Q_{11} decreases.

To understand this behaviour in the frequency domain, Fig.9b represents the adimensionalized pressure fluctuation spectra at these four operating conditions. As the computational domain is reduced, other phenomena such as the vortex rope are not captured here. Then these results only evaluate the impact of the inter-blade vortices on the runner.

As shown in the first part, while OP2 has only a small reverse flow vortex and a slight flow separation at the leading edge, OP3, OP4 and OP5 are characterized by developed inter-blade vortices. Figure 9b points out that these coherent vortices are generating high frequency torque fluctuations with similar amplitudes that almost five time lower at OP2. These high frequencies are generated by the small eddies shown in Fig. 6b. Moreover the different topologies observed at OP3, OP4 and OP5 does not affect considerably the amplitudes of the torque fluctuations; these vortices appear to generate a similar level of pressure fluctuations on the blades. The evolution of the standard deviation presented in Fig. 9b is actually controlled by the low amplitudes of the frequency phenomena. It can be concluded that inter-blade vortices generate fluctuations on a broad range of frequency in the runner channels when they are developed.

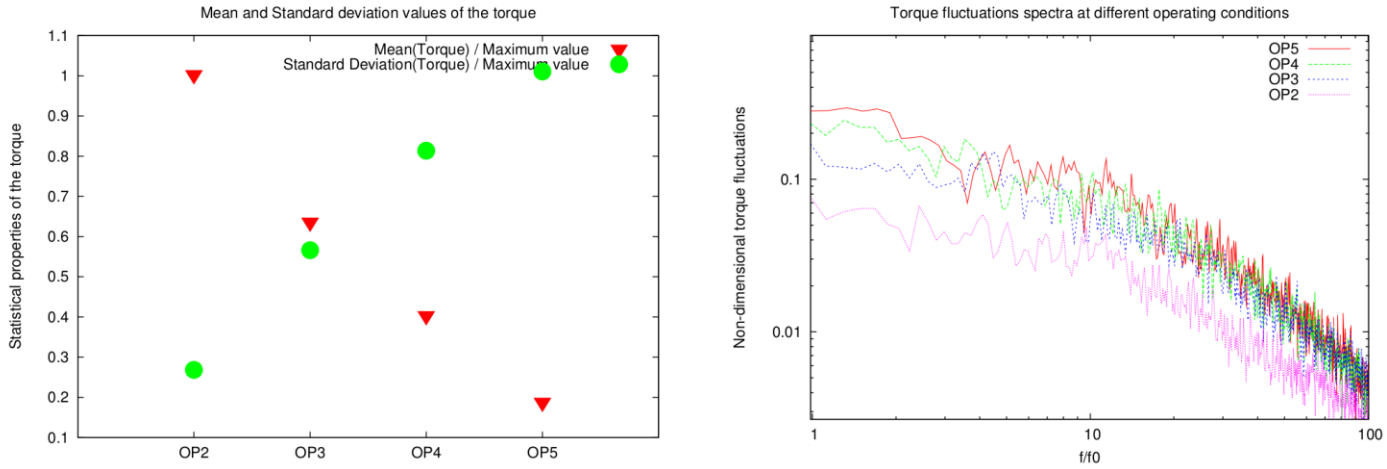

(a). Mean and RMS values of the torque

(b). Torque fluctuations spectra

Fig. 9 Influence of Q_{11} on the statistical properties and on the torque fluctuations spectrum.

4. Conclusion

It has been shown that RANS calculations on a simplified low head Francis turbine runner model are able to accurately predict the location and the topology of the inter-blade vortices. The vortices can be classified into four categories depending on their topologies and their driving phenomena. Each type corresponds to a flow regime which has been identified by their operating conditions. Highly resolved large eddy simulations lead to similar topologies with a higher level of detail. Large eddy simulations have been run to understand the pressure fluctuations generated by the inter-blade vortices. At a given Q_{11} value, it has been shown that pressure fluctuations increase when Q_{11} decreases. These pressure fluctuations are generated by the small eddies surrounding the vortices, which generate high pressure fluctuations, by the broad range of scale motion of the inter-blade vortices and by the unsteadiness of the reverse flow. These simulations where computed using a reduced domain and does not capture all the complex phenomena of these part load conditions. Further investigations have to be conducted in order to understand the interaction between the inter-blade vortices and other unsteady phenomena.

Acknowledgments

Computations presented in this paper were performed using HPC resources from GENCI (No. 020611). G.B. is also grateful for the support from Institut Universitaire de France.

References

[1] Doussot F, Balarac G, Brammer J, Métais O and Ségoufin C 2018 *29th IAHR Symp. on Hydraulic Machinery and Systems*
[2] Grunewald P and Diakonova M 2018 *Energy Research & Social Science* **38** 58–66
[3] Wack J and Riedelbauch S 2015 *Journal of Physics: Conf. Series* **656** 012074
[4] Zhou L, Liu M, Wang Z, Liu D and Zhao Y 2016 *28th IAHR Symposium on Hydraulic Machinery and Systems* **49** 1030–39
[5] Yamamoto K 2017 *Hydrodynamics of Francis turbine operation at deep part load condition* Ph.D. thesis Ecole Polytechnique Fédérale de Lausanne
[6] Zhou L, Liu M, Wang Z, Liu D and Zhao Y 2016 *Engineering Computations* **34** 364–376
[7] Bouajila S, De Colombel T, Lowys P and Maitre T 2016 *28th IAHR Symp. on Hydraulic Machinery and Systems* **49** 1010–19
[8] Bouajila S, Brammer J, Flores E, Ségoufin C and Maître T 2017 *Advances in Hydroinformatics* 931–945
[9] Zhang Y, Liu K, Xian H and Du X 2018 *Renewable and Sustainable Energy Reviews* **81** 1269 – 85
[10] Sagaut P and Meneveau C 2006 Large Eddy *Simulation for Incompressible Flows: An Introduction* Scientific Computation (Springer) ISBN 9783540263449 URL : *https://books.google.fr/books?id=ODYiH6RNyoQC*
[11] Guedot L, Lartigue G and Moureau V 2015 *Physics of Fluids* **27** 045107